2582–2588 *Nucleic Acids Research, 1997, Vol. 25, No. 13*

Visualization of RNA crystal growth by atomic force microscopy

Joseph D. Ng, Yurii G. Kuznetsov[1], Alexander J. Malkin[1], Gérard Keith, Richard Giegé* and Alexander McPherson[1]

Unité Propre de Recherche 'Structure des Macromolécules Biologiques et Mécanismes de Reconnaissance', Institut de Biologie Moléculaire et Cellulaire du Centre National de la Recherche Scientifique, 15 rue René Descartes, F-67084 Strasbourg Cedex, France and [1]University of California, Riverside, Department of Biochemistry, Riverside, CA 92521, USA

Received April 7, 1997; Accepted April 28, 1997

ABSTRACT

The crystallization of transfer RNA (tRNA) was investigated using atomic force microscopy (AFM) over the temperature range from 4 to 16°C, and this produced the first *in situ* AFM images of developing nucleic acid crystals. The growth of the (110) face of hexagonal yeast tRNA^{Phe} crystals was observed to occur at steps on vicinal hillocks generated by multiple screw dislocation sources in the temperature range of 13.5–16°C. Two-dimensional nucleation begins to dominate at 13.5°C, with the appearance of three-dimensional nuclei at 12°C. The changes in growth mechanisms are correlated with variations in supersaturation which is higher in the low temperature range. Growth of tRNA crystals was characterized by a strong anisotropy in the tangential step movement and transformation of growth modes on single crystals were directly observed by AFM over the narrow temperature range utilized. Finally, lattice resolution images of the molecular structure of surface layers were recorded. The implications of the strong temperature dependence of tRNA^{Phe} crystal growth are discussed in view of improving and better controlling crystallization of nucleic acids.

INTRODUCTION

The theoretical bases describing the growth mechanisms and pathways of macromolecular crystals resemble those of conventional molecules (1–3). However, in practice, the crystal growth phenomena of proteins significantly differ in their kinetic and thermodynamic properties. In particular, protein crystals nucleate at extremely high levels of supersaturation and have relatively slow growth rates. These facts, in general, are correlated with the higher complexity in composition, structure, surface features and surface potential of macromolecules. Moreover, protein crystals have very high solvent contents and exhibit less lattice interactions compared with small molecule crystals. Significant efforts have been recently undertaken to study the physics of surface processes during the crystal growth of a few protein and virus crystals (from the point of view of crystal growth, viruses will be considered equally as proteins in this study, because their nucleic acid components are inside the protein capsids), amenable to interferometric techniques (4–8), electron microscopy (9,10), X-ray topography (11,12) and atomic force microscopy (13–21). It was shown that macromolecules utilize in their crystallization the same growth mechanisms and contain the same kinds of defects as inorganic crystals (22,23). These include growth on dislocations, two- and three-dimensional nucleation and a variety of faults involving inclusion, point, linear and planar defects described already for a variety of different macromolecular crystals.

In comparison with proteins very few nucleic acid molecules, especially RNAs have been crystallized (24). Moreover, in exception to small oligonucleotide crystals, most other RNA crystals so far obtained are of rather limited quality and diffract to only low or moderate resolution, with only a few exceptions diffracting better than 3.0 Å (e.g. 25–30), so that only a few RNA structures of 'globular' type could be solved by X-ray diffraction analysis. The difficulties encountered in RNA crystallization certainly rely on the preparation of adequate RNA samples, but probably also to particular features of the nucleic acid crystal growth process. With the development of RNA production techniques the first bottleneck has been essentially overcome and as a consequence significant progress in the crystallization of RNAs has occurred recently (31). However, producing such crystals still remains a difficult and empirical task, since no specific background on the growth mechanisms of nucleic acid crystals is available that could guide crystal growers. Indeed, almost nothing is known about growth mechanisms, kinetics of growth, development of surface morphology or growth defects of nucleic acid crystals.

In this work, using yeast phenylalanine transfer RNA (tRNA-^{Phe}) as a model, we examined for the first time the generation of the surface morphology on an RNA crystal under different experimental conditions. Visualization of the growth phenomena was made *in situ* by AFM on growing crystals. Experiments were

* To whom correspondence should be addressed. Tel: +33 3 88 41 70 58; Fax: +33 3 88 60 22 18; Email: giege@ibmc.u-strasbg.fr

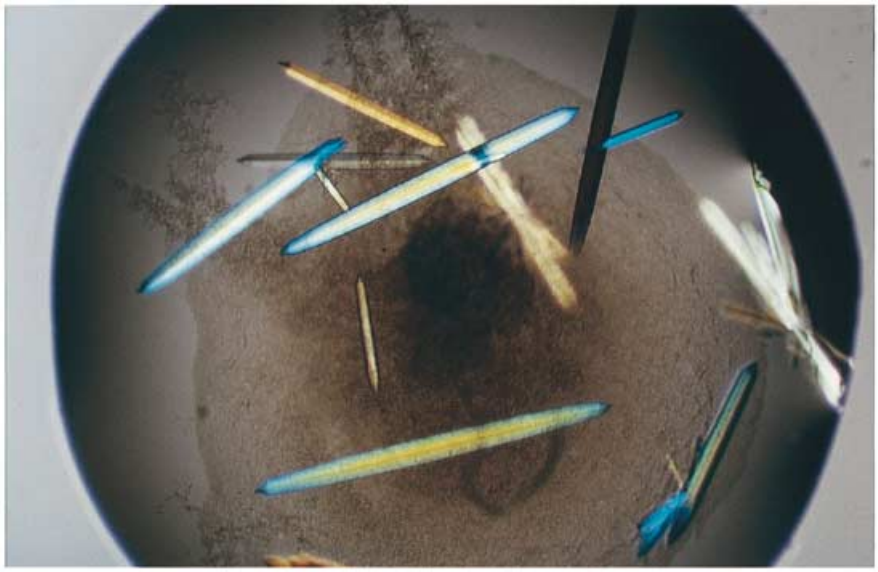

Figure 1. Hexagonal $tRNA^{Phe}$ crystals nucleated on etched glass substrates. Growth occurred in the presence of 15% MPD by vapor phase diffusion as described in Materials and Methods. AFM measurements were performed on crystals having 0.2–0.4 mm in the longest dimensions.

conducted in such a way that the supersaturation of the crystallizing solution could be varied by temperature shifts during the growth process and growth kinetics could also be observed. As for proteins, different growth mechanisms could be seen depending on the supersaturation level of the crystallizing solutions. It was observed that the growth of tRNA crystals is sensitive to variations of supersaturation conditions as modulated by temperature and that different modes of growth can occur sequentially on the same crystal. The implications of these observations for the preparation of better RNA crystals and the design of more efficient crystallization protocols are discussed.

MATERIALS AND METHODS

Preparation of $tRNA^{Phe}$

The tRNA used in this study was purified to homogeneity from brewer's yeast using a two step procedure as described by Keith and Dirheimer (32) involving counter-current distribution (33) and benzoylated DEAE–cellulose chromatography (34). The purity of the $tRNA^{Phe}$ was evaluated by one- and two-dimensional polyacrylamide gel electrophoreses (35) and tRNA aminoacylation assays (32).

Crystallization and X-ray analysis of $tRNA^{Phe}$

Purified yeast $tRNA^{Phe}$ was dialyzed against sterile water for 2 days and a final working concentration of 6 mg/ml was prepared with a centricon-10 concentrator (Amicon, Inc., MA). Crystallization was performed by sitting drop vapor diffusion methods (36). A 20 µl solution consisting of 10 µl RNA solution and 10 µl crystallizing solution was prepared on an etched glass substrate in a sealed 90 mm diameter Petri dish and equilibrated overnight against 25 ml of crystallizing solution containing 15% MPD (2-methyl-2,4-pentanediol), 100 mM sodium cacodylate (pH 6.5), 20 mM $MgCl_2$, 2 mM $CoCl_2$ and 2 mM spermine. Nucleation and growth conditions were recorded in the 4–18°C temperature range.

Crystals were mounted in thin-walled glass capillaries for diffraction analysis at 4°C. X-ray data were collected on a 30 cm diameter MAR Research image-plate detector system with a Rigaku RU-200BH rotating anode X-ray generator with a Huber graphite monochromator operating at 50 kV and 80 mA. Direct monochromatic measurements were performed with the X-ray beam perpendicular to the long axis of the crystal. Data were collected at oscillation ranges of 0.5° with 5° crystal rotation at 30 s exposure per frame. Diffraction measurements were repeated for each of the same crystal at an orientation change of 90°.

AFM techniques

Seed crystals of tRNA were nucleated and grown on glass substrates in a droplet of 6 µl by vapor diffusion method consisting of 6 mg tRNA/ml water mixed with an equal volume of crystallizing solution. The glass substrates with seed crystals were carefully transferred into a sealed fluid cell of a Digital NanoScope E (Digital Instruments, Santa Barbara, CA) atomic force microscope. The entire volume of the cell was ~50 µl filled with a mixture of mother liquor containing 1.0 mg/ml of RNA, 15% MPD, 100 mM sodium cacodylate (pH 6.5), 20 mM $MgCl_2$, 2 mM $CoCl_2$ and 2 mM spermine. Images were collected in contact mode using an oxide sharpened tip from Park Scientific Instruments (Sunnyvale, CA). Cantilevers with nominal force constants of 0.01 N/m were typically applied. In order to minimize the force applied to the crystalline surface during the scanning, the set point voltage was continually adjusted to the lowest level for which tip-crystal contact was maintained. The solution temperature in the fluid cell was modulated by a MI 1012 thermoelectric cooler (TEC) (Marlow Industries Inc., Dallas, TX). Temperature control of TEC were provided by a temperature controller SE 5000 (Marlow Industries Inc). Supersaturation conditions were exclusively modulated by temperature changes. The mother liquor for crystal growth remained the same in all

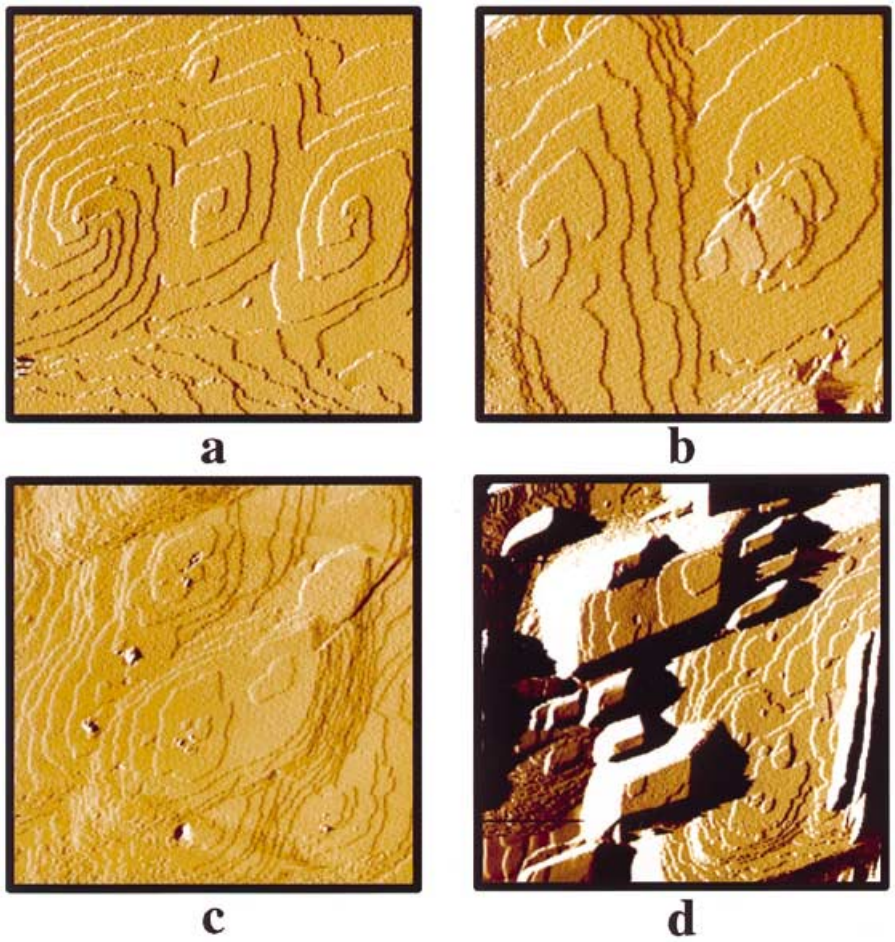

Figure 2. Different surface morphologies of yeast $tRNA^{Phe}$ crystals seen at different temperature ranges on various locations of the crystal face. (**a**) Dislocation hillocks are formed at 15°C by multiple right handed (left side of image), single left handed (center of image) and double right handed screw dislocations (right side of image). (**b**) Development of a double and single screw dislocation at 14°C. The edges of the growth steps are very rough indicative of high level impurities present in the crystallizing solution that can potentially incorporate into the crystal. (**c**) Growth by 2D nucleation at 13°C showing growth and coalescence of islands and expansions of stacks. Formation of a hole caused by incorporation of foreign particles during growth of additional layers are shown in the bottom center of the image. (**d**) Dominant mechanism of growth is by 3D nucleation with multilayer stack macrostep production at 12°C. Scan areas for the images are (a and b) $23 \times 23\ \mu m^2$, (c) $20 \times 20\ \mu m^2$ and (d) $34 \times 34\ \mu m^2$.

AFM experiments. Because of the small amount of material available to us, it was not possible to ascertain the exact degrees of supersaturation at which particular growth rates occurred.

RESULTS

$tRNA^{Phe}$ crystals used for AFM measurements

The $tRNA^{Phe}$ proved to be a practical molecule for this investigation due to its wide range of crystallization conditions and sensitivity to small temperature changes. This $tRNA^{Phe}$ can be crystallized in 12 different crystal forms under various conditions (reviewed in 25). We have chosen crystallization conditions that produce the hexagonal habit using MPD as the principle crystallizing agent since crystals of this form were the fastest and easiest to obtain. In addition, $tRNA^{Phe}$ crystals of this habit were most technically feasible for our AFM studies in that single seed crystals can be easily oriented and positioned for scanning. Finally with these crystals, it is easy to modulate supersaturation, the crystallization driving force, by temperature shifts without any other changes in solution conditions. Indeed the hexagonal $tRNA^{Phe}$ crystals nucleated at 4°C, can grow in the 4–16°C temperature range. We have verified that supersaturation increases when temperature decreases. This was done by estimating the number of nuclei appearing in solution which is highest at the lowest temperature. This fact is further supported by observations made on the crystal surfaces showing an increase of both 2D nucleation and tangential step rates at decreasing temperatures.

Hexagonal crystals measuring up to 0.6 mm in their longest dimensions can be obtained at 4°C overnight under the conditions specified here (Fig. 1). tRNA crystals obtained were of hexagonal habit having space group $P6_222$ with a = b = 82 Å, c = 236 Å, and $\alpha = \beta = 90°$, $\gamma = 120°$. In our hands, the maximum resolution to which X-ray data can be collected, varied between 4.0 and 6.0 Å for the crystals used in our AFM studies.

Different surface morphologies of $tRNA^{Phe}$ crystal

Figure 2 displays images representative of many recorded over the temperature range investigated and illustrates the mechanisms responsible for the generation of growth steps on different regions

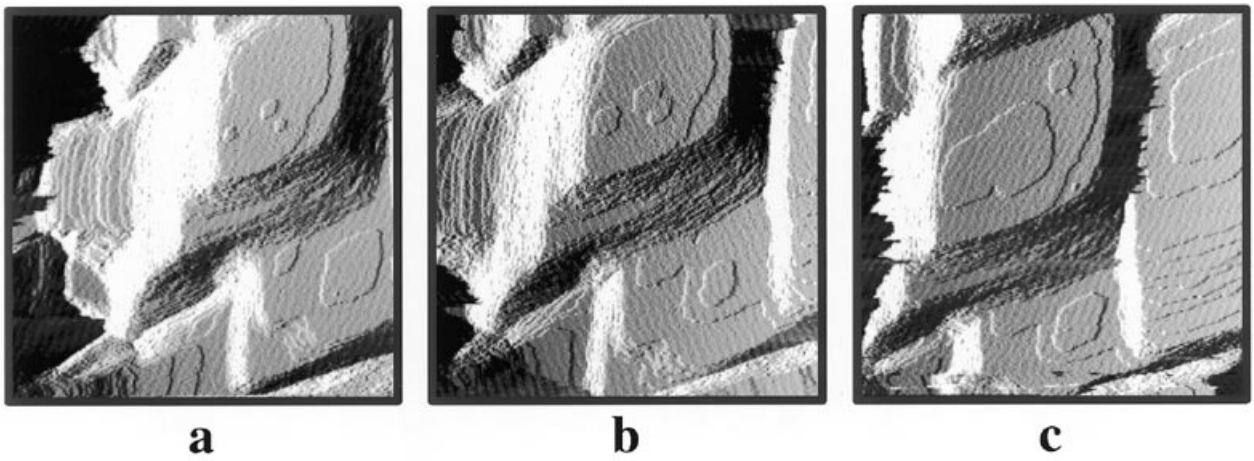

Figure 3. Visualization of growth kinetics. (a–c) *In situ* AFM images of a $20 \times 20\ \mu m^2$ scan area of the surface of a growing $tRNA^{Phe}$ crystal recorded at times $t = 0$ (**a**), $t = 6$ min (**b**) and $t = 12$ min (**c**).

of crystal surfaces. In the temperature range between 13.5 and 16°C, the growth of RNA crystals occurs in steps on steep vicinal hillocks with the slope $p = 10^{-2}$ [where p = tan(angle of slope of vicinal hillocks)], generated by screw dislocation sources. The step heights were 90 ± 5 Å, corresponding to the unit cell dimension of the hexagonal $tRNA^{Phe}$ crystal. Dislocation hillocks are typically observed on the surfaces of RNA crystals and they are formed by both right and left handed single, double or multiple dislocations (Fig. 2a and b). Most of the observed dislocation sources were developed in the seed during the nucleation period at 4°C. However, formation of new dislocation sources were seen upon incorporation of debris particles or precipitate into the growing crystal. At the temperature range, 12–13.5°C, the tRNA crystal grow by 2D nucleation (Fig. 2c). Visualization of a growing crystal surface at ≤12°C, reveals that growth by 3D nucleation becomes the dominant mechanism. Multilayer stacks, which grew both tangentially and in the normal direction were formed on the crystalline surface (Fig. 2d).

Figure 3a–c records the progression of growth steps and the development of 2D nuclei at 6 min intervals over a period of 12 min. On the plateaus of high, steep, multilayer stacks, 2D islands appear and can be seen to extend tangentially, as do the step edges comprising the slopes of the hillocks themselves. From measurements of the rate of movement of step edges at different supersaturations and temperatures, an estimate of the fundamental kinetic parameters can be obtained. The range of the growth rate is approximately $v = 1.25 \times 10^{-8}$ cm/s (at 15°C) to $v = 13.0 \times 10^{-8}$ cm/s (at 12.4°C).

Dynamic morphological changes on the crystal surface as a function of temperature

In the temperature range of 16–11°C, transition from one growth mechanism to another was observed on a single location of the crystal surface. As exemplified in Figure 4, at ~14°C, the shape of the growth spirals became increasingly isotropic and 2D nuclei began to appear. The dislocation hillocks then became less pronounced as 2D nucleation assumed dominance. At 12°C, 3D nuclei began to appear on the crystal surface giving rise to large, multilayer stacks of steps. The effect of temperature was, in fact, so dominant for the tRNA crystals that they were readily dissolved by raising the temperature >16°C and regrown many times in a cyclic, reversible fashion by then lowering the temperature.

High resolution image

It was possible to obtain lattice resolution images of the tRNA crystals as presented in both unprocessed and Fourier filtered form in Figure 5. The cell constants of the lattice were consistent with the expected spacings on the [110] face of the hexagonal crystal, but the images did not contain molecular features characteristic of tRNA. We believe, however, that refinements in the AFM technique may ultimately allow us to observe molecular level details.

DISCUSSION

Direct visualization of crystal growth

Atomic force microscopy performed on a single yeast $tRNA^{Phe}$ crystal revealed several classes of defects that are in common with those observed for protein crystals. The images indicate that $tRNA^{Phe}$ crystals grow either by 2D nucleation on surfaces or on steps by the development of screw and multiple screw dislocations, as well as by 3D nucleation by multilayer stack macrostep production. The dislocation and imperfection are formed during crystal growth upon adsorption and incorporation of impurities such as macromolecular aggregates, contaminating proteins or dust particles. Incorporation of foreign particles often results in a formation of a hole that persist upon growth of additional layers (Fig. 2c). These holes were equally observed in lysozyme (15), canavalin (16) and satellite tobacco mosaic virus crystals (18,37). Similar to proteins, growth by 3D nucleation dominates at high supersaturation.

Importantly, tRNA crystals demonstrated a remarkable sensitivity to temperature variation. When supersaturation is increased as the temperature is reduced there can be a striking transition from one growth mechanism to another (Fig. 4). This sensitivity to temperature was also evidenced by variations of the growth

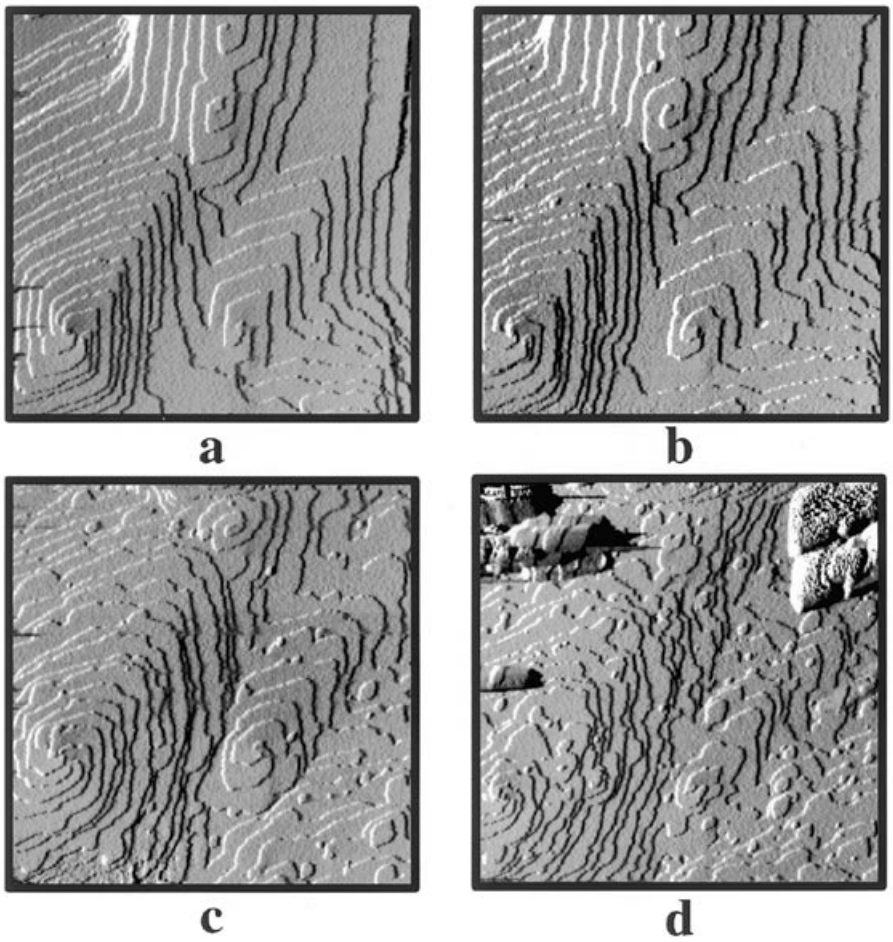

Figure 4. Dynamic changes in growth morphologies induced by temperature changes. (a–d) Successive AFM images of a 30× 30 μm^2 scan area of the surface of a growing yeast tRNA^{Phe} crystal recorded at times (**a**) t = 0 s, (**b**) t = 2 h, (**c**) t = 3.25 h and (**d**) t = 4.25 h. In the interval between each recording, the temperature was reduced from 16°C in (a) to 14°C in (b), to 12°C in (c), and to 11°C in (d). Particularly noteworthy is the change in shape of growth spirals from roughly rectangular to nearly circular shapes as the temperature is lowered and, consequently, the supersaturation is increased. Over the period of the four observations, the mechanism of growth transforms from one relying almost exclusively on screw dislocation sources in (a), to one dominated by the appearance of 2D nuclei in (c), and especially in (d), where stacks of layers are seen in the upper right corner.

rates by two order of magnitude in a temperature window of <3°C (between 12.4 and 15°C).

The 3D nuclei appearing on the growing crystal surfaces are of unique interest because they appear to form from large noncrystalline clusters that become crystalline upon contact with the surface lattice. Generally these nuclei assume an orientation consistent with the crystal lattice and give rise to macrosteps that contribute coherently to the overall crystal. In some cases, however, large, misoriented 3D nuclei were observed. Because the crystals we studied were nucleated at 4°C, this mechanism was likely responsible for their initial dislocation structure.

High resolution images provided molecular-scale contrast that revealed lattice parameters and polymorph identification while simultaneously enabling real-time observation of growth modes and assessment of crystal quality.

Growth conditions may affect diffraction properties

Previous AFM studies of protein crystals have revealed different defect structures and densities (21). The hexagonal tRNA crystals grown at 4–11°C in this study (high supersaturations) diffract to 6 Å resolution under a conventional X-ray source. We speculate at this point, in a qualitative sense, that there is a correlation between growth conditions and diffraction properties. For example at 11°C there is a continuous flux of 3D nuclei, some of them being misoriented microcrystal forms, incorporating into the bulk crystal (Fig. 3d). Such RNA crystals are therefore grown under a stress state which may result in splitting or widening of Bragg reflections and a decrease in diffraction properties as shown for inorganic crystals (3). In support of this view, we have observed that tRNA^{Phe} crystals grown under the same conditions at 15°C having lower supersaturation, have more regular surface morphology (Fig. 3c) and these crystals diffract to 4 Å.

The question remains as to how AFM images may guide us to choose crystal growth conditions for obtaining maximum statistical order of RNA crystals, to give higher diffracting or better quality crystals. The notion that excessive supersaturation required for nucleation for macromolecules gives rise to unfavorable conditions for crystal growth is supported by the observation in the small molecule field that a higher frequency of defects is observed at higher supersaturation conditions (3). In the case of tRNA^{Phe},

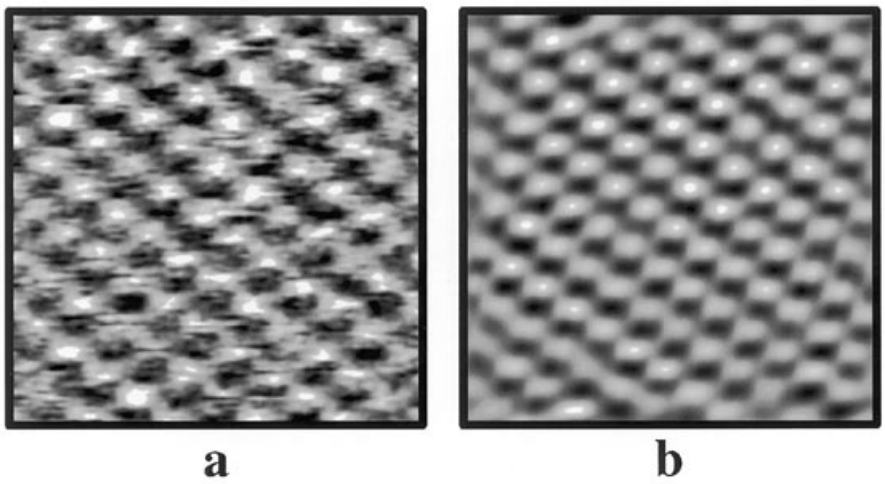

Figure 5. High resolution view of the [110] surface of a $tRNA^{Phe}$ crystal. An unprocessed 800×800 nm^2 AFM image of the surface of a growing crystal is shown in (**a**), and the same image after Fourier filtering in (**b**).

even subtle increases in supersaturation by decreasing temperature lead to significantly less orderly growth with mixed modes of step generation. This suggests that crystals of greater internal order might well be attainable if growth is maintained at an optimal and constant level of supersaturation. The sensitivity to supersaturation changes, being more prominent in RNA crystals than in other macromolecular crystals, may explain in part the difficulties encountered in crystallizing RNA molecules.

The intrinsic order of a crystal lattice is often discussed in terms of mosaicity. In crystals of conventional materials the rocking curves and the peak centers of Bragg reflections are indeed dependent on the crystal defect density (38). Presently, such studies are extremely sparse in the protein field and completely absent for nucleic acids. Even though we have not yet made the direct correlation between mosaic spread and defect structure with the $tRNA^{Phe}$ crystals, we predict that the corresponding properties for RNA and protein crystals may be similarly correlated. Improvement of mosaicity in microgravity-grown lysozyme (39) and thaumatin (40) crystals, where growth conditions are more regular with minimized flow convection, have already shown improved diffraction intensity and limit. We plan to examine mosaic spread of RNA crystals on synchrotron facilities and to correlate it with differences in growth mechanisms as visualized by AFM.

Perspectives on RNA crystallization

Crystallization features in the RNA field have been best studied for tRNAs. To date more than 17 tRNA species have been surveyed for crystallization (reviewed in 25). We discuss here some general trends and how they may be related to observations in real-time visualization of the crystal surface of $tRNA^{Phe}$.

Very frequently nucleation of tRNA crystals occurs in a precipitated environment followed by the maturation of a crystal with a concomitant disappearance of precipitation. Even though this phenomenon is not unique to RNA molecules (41), the success of many tRNA crystallizations has been attributed to driving crystal growth from slightly precipitated and turbid solutions (25). This implies that tRNA crystal growth has traditionally been achieved in very high supersaturation environments where crystal defects may occur by 3D nucleation or incorporation of foreign particles. In this case, included particles principally cause lattice strain in the immediate proximity of the incorporated element. Thus the overall mechanical and diffraction properties of the crystal is weakened or impaired.

Crystalline polymorphism is more pronounced with tRNA than with most protein molecules. For example, with yeast $tRNA^{Phe}$, 12 different space groups have been characterized (reviewed in 25). In addition different tRNAs, as yeast $tRNA^{Leu}$ or $tRNA^{Asp}$, can even crystallize from the same mother liquor under different crystal forms (25). The outstanding characteristic of tRNA polymorphism is principally attributed to a high variability in intermolecular packing, to conformational flexibility, and to its polyelectrolyte nature (25). In addition, RNA is naturally more unstable than other biological polymers due to the presence of the free 2′-hydroxyl group on the ribose moieties. Internal cyclization of these hydroxyl groups can occur with neighboring phosphates leading to molecular breakdown products within a crystal unit as observed in $tRNA^{Asp}$ crystals (42). These features may directly lead to statistical misalignment about mean lattice points and structural heterogeneity of the molecules.

Historically, unexplained observations in tRNA crystallography revealed frequent occurrence of soft and extremely fragile crystals having limited diffraction qualities accompanied by seldom mechanically robust crystals diffracting at higher resolution. Most RNA crystals are mechanically fragile due to their high solvent content. We have observed that under higher supersaturation conditions, the surface of a growing $tRNA^{Phe}$ crystal is more sensitive to lateral shear forces imposed by the scanning probe during imaging.

tRNA crystals exhibit a great irregularity in their diffraction ability. In the case of $C222_1$ crystals of yeast $tRNA^{Asp}$, the diffraction limit is usually 4 Å sometimes reaching 3 Å and in exceptional cases, 2.5 Å (25). These crystals are often characterized by asymmetric diffraction spots reflecting lattice disorders. The principal reason for crystalline disorder has been linked to the inherent structural flexibility of nucleic acids due to the great number of rotatable bonds in the ribose–phosphate backbone.

The intrinsic flexibility of the nucleic acid ultrastructure has much higher degrees of freedom than that of proteins where flexibility is based primarily on simple inter-peptide bonds. Perhaps the most compelling feature correlating to internal disorder for tRNA crystals is its tendency to exhibit strong thermal diffuse scattering (25) resulting in severe distortion of the reciprocal lattice. We have observed in precession diffraction patterns of $tRNA^{Phe}$ crystals grown at higher supersaturation distinct distorted diffraction spots at the higher resolution limits (unpublished).

In considering these unique characteristics of tRNA crystal growth coupled with what we can observe by AFM, we may consider the practical application of real-time visualization of nucleation and growth in regards to identifying polymorphs, examining the role of aggregates and defects, and correlating diffraction properties of RNA crystals with their defect structure. Further studies will entail the evaluation of X-ray diffraction data from crystals of known defect structure established by AFM.

In conclusion, an immediate practical consequence of the present investigation is the insight for designing more efficient crystallization protocols for the growth of higher quality RNA crystals. An obvious approach would be to reduce supersaturation after the nucleation step, so that the crystal growth would occur by regular and unique mechanisms. However, care should be taken to avoid conditions where growth switches frequently from one growth mode to another as the result of supersaturation fluctuations. Control over temperature and limiting supersaturation windows may avoid such effects.

ACKNOWLEDGEMENTS

We thank A.Ducruix (Gif-sur-Yvette) for help in X-ray diffraction measurements, A.Greenwood (Riverside) for his technical assistance during the AFM studies and B.Lorber for his helpful discussions. This research was supported by grants from the National Aeronautics and Space Administration, the Center National d'Études Spatiales (CNES) and the Centre National de la Recherche Scientifique (CNRS). J.D.N. was supported by CNES and NATO fellowships.

REFERENCES

1 Burton,W.K., Cabrera,N. and Frank,F.C. (1951) *Phil. Trans. R. Soc. London*, **A243**, 99–125.
2 Boistelle,R. and Astier,J.-P. (1988) *J. Crystal Growth*, **90**, 14–30.
3 Chernov,A.A. (1997) *J. Crystal Growth*, in press.
4 Vekilov,P.G. (1993) *Prog. Cryst. Growth Charact. Materials* **26**, 25–49.
5 Komatsu,H., Miyashita,S. and Suzuki,Y. (1993) *Jpn. J. Appl. Phys.*, **32**, L1855–1857.
6 Vekilov,P.G., Ataka,M. and Katsura,T. (1993) *J. Crystal Growth*, **130**, 317–320.
7 Kuznetsov,Y.G., Malkin,A.J., Greenwood,A. and McPherson,A. (1995) *J. Struct. Biol.*, **114**, 184–196.
8 Rosenberger,F., Vekilov,P.G., Muschol,M. and Thomas,B.R. (1996) *J. Crystal Growth*, **168**, 1–27.
9 Durbin,S.D. and Feher,G. (1990) *J. Mol. Biol.*, **212**, 763–774.
10 Devaud,G., Furcinitti,P.S., Fleming,J.C., Lyon,M.K. and Douglas,K. (1992) *Biophys. J.*, **63**, 630–638.
11 Stojanoff,V. and Siddons,D.P. (1996) *Acta Cryst.*, **A52**, 498–499.
12 Fourme,R., Ducruix,A., Riès-Kautt,M. and Capelle,B. (1995) *J. Synchrotron Rad.*, **2**, 136–142.
13 Durbin,S.D. and Carlson,W.E. (1992) *J. Crystal Growth*, **122**, 71–79.
14 Littke,W. and Haber,M. (1992) *J. Crystal Growth*, **122**, 80–86.
15 Konnert,J.H., D'Antonio,P. and Ward,K.B. (1994) *Acta Cryst.*, **D50**, 603–613.
16 Land,T.A., Malkin,A.J., Kuznetsov,Yu.G., McPherson,A. and DeYoreo,J.J. (1995) *Phys. Rev. Letts*, **75**, 2774–2777.
17 Malkin,A.J., Land,T.A., Kuznetsov,Yu.G., McPherson,A. and DeYoreo,J.J. (1995) *Phys. Rev. Letts*, **75**, 2778–2781.
18 Malkin,A.J., Kuznetsov,Yu.G., Land,T.A., DeYoreo,J.J. and McPherson,A. (1995) *Nature Struct. Biol.*, **2**, 956–959.
19 Malkin,A.J., Kuznetsov,Y.G., Glantz,W. and McPherson,A. (1996) *J. Phys. Chem.*, **100**, 11736–11743.
20 Yip,C.M. and Ward,M.D. (1996) *Biophys. J.*, **71**, 1071–1078.
21 Malkin,A.J., Kuznetsov,Y.G. and McPherson,A. (1996) *J. Struct. Biol.*, **117**, 124–137.
22 Chernov,A.A.(1984) *Modern Crystallography III. Crystal Growth.* Springer, Berlin & New York.
23 Krasinlki,M.J. and Rolandi,R. (1996) *J. Crystal Growth* **169**, 548–556.
24 Gilliland,G.L. and Ladner,J.E. (1996) *Curr. Opin. Struct. Biol.*, **6**, 595–603.
25 Dock,A.-C., Lorber,B., Moras,D., Pixa,G., Thierry,J.-C. and Giegé,R. (1984) *Biochimie*, **66**, 179–201.
26 Doudna,J.A., Grosshaus,C., Gooding,A. and Kundrot,C.E. (1993) *Proc. Natl. Acad. Sci. USA*, **90**, 7829–7833.
27 Pley,H.W., Lindes,D.S., DeLuca-Flaherty,C. and McKay,D.B. (1994) *J. Biol. Chem.*, **263**, 19656–19658.
28 Scott,W.G., Finch,J.T., Grenfell,R., Fogg,J., Smith,T., Gait,M.J. and Klug,A. (1995) *J. Mol. Biol.*, **250**, 327–332.
29 Wahl,M.C., Ramakrishnan,B., Ban,C., Chen,X. and Sundaralingam,M. (1996) *Acta Crystallogr.*, **D52**, 668–675.
30 Ott,G., Dörfler,S., Sprinzl,M., Müller,U. and Heinemann,U. (1996) *Acta Crystallogr.*, **D52**, 871–873.
31 Lietzke,S.E., Barnes,C.L. and Kundrot,C.E. (1995) *Curr. Op. Struct. Biol.*, **5**, 645–649.
32 Keith,G. and Dirheimer,G. (1987) *Biochem. Biophys. Res. Commun.*, **147**, 183–187.
33 Dirheimer,G. and Ebel,J.-P. (1967) *Bull. Soc. Chim. Biol.*, **49**, 1679–1687.
34 Gillam,I., Millward,S., Blew,D., vonTigerstrom,M. and Wimmer,E. (1967) *Biochemistry*, **6**, 3043–3056.
35 Keith,G. (1990) Chromatography and modification of nucleosides (chapter 3) *J. Chromatography Library.* Elsevier **45A**, A103–A141.
36 Ducruix,A. and Giegé,R. (eds) (1992) *Crystallization of Nucleic Acids and Protein, A Practical Approach.* IRL Press, Oxford, UK.
37 Malkin,A.J., Kuznetsov,Yu.G. and McPherson,A. (1996) *Proteins*, **24**, 247–252.
38 Helliwell,J.F. (1992) *Macromolecular Crystallography with Synchrotron Radiation.* Cambridge University Press, Cambridge, UK.
39 Weisgberber,S. and Helliwell,J.R. (1995) *Acta Crystallogr.*, **D51**, 1099–1102.
40 Ng,J.D., Lorber,B., Giegé,R., Koszelak,S., Day,J., Greenwood,A. and McPherson,A. (1997) *Acta Crystallogr.* in press.
41 Ng,J.D., Lorber,B., Witz J., Théobald-Dietrich,A., Kern,D. and Giegé,R. (1996) *J. Crystal Growth*, **168**, 50–62.
42 Moras,D., Dock,A.-C., Dumas,P., Westhof,E., Romby,P., Ebel,J.-P. and Giegé,R. (1985) *J. Biomol. Struct. Dyn.*, **3**, 479–493.